Anisotropy of excited He^+ formed in the photoionization of helium

Hossein R. Sadeghpour and Chris H. Greene
Department of Physics and Astronomy, Louisiana State University, Baton Rouge, Louisiana 70803
(Received 13 July 1988)

Semianalytic methods are developed to predict the alignment and orientation of excited helium ions produced in the photoionization of neutral helium in the low-energy limit. The ionic electron probability distribution is shown to align itself orthogonal to the direction of the incident light polarization axis in the same manner as the photoelectron angular distribution [C.H. Greene, Phys. Rev. Lett. **44**, 869 (1980)]. In certain instances, propensity rules for the alignment and orientation of the ionic electron are violated. Coherent contributions from different degenerate orbital angular momenta are seen to be partially responsible for these "unfavored" trends. Explicit predictions of the time-unresolved fluorescence polarization are presented, including the effects of fine-structure depolarization.

I. INTRODUCTION

Theoretical investigation of photofragmentation anisotropy has mainly focused on the angular distribution of photofragments[1] and on the first and second rank multipole moments of the total "collision-fragment" angular momentum tensor. Fano and Macek[2] demonstrated that these two multipole moments, termed orientation and alignment, respectively, can be extracted by measuring the intensity of polarized fluorescence from a specific fragment state. Greene and Zare[3] adapted the angular momentum transfer formulation of Dill and Fano[1,4] to cast the orientation and alignment parameters in the same form as the photofragment asymmetry parameter β, as incoherent sums over angular momentum transfer channels.

The analysis of Ref. 1 showed that for the parity-unfavored class of electric dipole transitions, the value $\beta_{\rm unf}=-1$ automatically results, corresponding to emission of the photofragment orthogonal to the incident light polarization axis. Parity-favored transitions, on the other hand, were shown to "normally" have a positive asymmetry parameter, implying ejection of the photofragment predominantly in the direction of the polarization vector of the incident light. In the first application of the formalism of Ref. 1 to two-electron systems, H^- or He, Greene[5] demonstrated nevertheless that for certain parity-favored processes, the photoelectron is ejected from H^- (or He) in a sideways fashion ($\beta\rightarrow -1$) leaving behind an unobserved hydrogenic fragment in one of its degenerate excited states. The crosswise ejection of photoelectrons was qualitatively associated with the action of Herrick's[6] SO(4) Casimir operator $T^2=(\mathbf{L}\cdot\hat{\mathbf{r}}_e)^2$, where L is the total angular momentum of the two-electron system and $\hat{\mathbf{r}}_e$ is the unit vector along the photoelectron escape axis. Nonzero values of T, the projection of the inner electron angular momentum l_i onto the photoelectron escape axis, reflect some type of torque action on the photoelectron by the unobserved electron's angular momentum. In this paper we extend the treatment of Ref. 5 to describe properties of the residual ionic fragment, He^+ ($n\geq 2$), by casting the electronic probability density into the same form as the photoelectron angular distribution.

The typical photofragmentation experiment involves photoionization of a neutral atom, accompanied by excitation of the residual ion into a specific angular momentum state l_i. Photoexcitation of two-electron systems such as He or H^- into residual hydrogenic states of high quantum numbers, on the other hand, presents additional complications. The "accidental" degeneracy, in l_i, of the nonrelativistic one-electron energy spectrum ensures that the parity allowed quantum pathways for the transitions of these collision-excited orbital momentum states interfere coherently. The effect of this coherence, hereafter called l_i coherence, on the Fano-Macek[2] analysis of fluorescence polarization has recently been investigated.[7,8] Burgdörfer's[8] group-theoretical reformulation of the hydrogenic density matrix gives these parameters in terms of expectation values of spherical tensor operators constructed by coupling the hydrogenic constants of motion operators, the angular momentum **L**, and the Runge-Lenz vector **A**. The calculation of these pseudospin multipoles and their eventual inverse transformation, recoupling into multipoles of **L** and **A**, becomes increasingly complicated for high-lying states as pointed out by Burgdörfer. In this paper we investigate the effects of l_i coherence on the alignment and circulation (orientation) of the ionic electron probability distribution from a more pedestrian perspective which allows, in principle, for the calculation of these parameters for very high principal quantum numbers. The derivation follows that of Fano and Macek, in spirit, but with substantial differences associated with the coherence in l_i.

The use of a simple asymptotic final-state wave function[5] which incorporates the correlation between the ionic electron and the ejected photoelectron in terms of a Gailitis-Damburg-type[9] eigenvector allows us to study the behavior of the anisotropy parameters for states of $He^+(nl_i)$ with $n\geq 2$. This analysis offers a quantitative method for making predictions about the anisotropy parameters without requiring elaborate variational calcula-

tions of the type conducted recently by Hayes and Scott.[10] Empirical evidence for the validity of such a simplification will be provided below in Sec. II A.

II. THEORY AND DISCUSSION

A. Final-state wave function

Upon photoionization of the He ground state, the residual ion He^+ is left in an excited state, $n \geq 2$. These excited nl_i states of the hydrogenic ion $He^+(n)$ with different l_i can be regarded as degenerate. (Effects of the very small splitting of these levels are discussed in Sec. II D.) This "accidential" degeneracy is responsible for the formation of a permanent electric dipole moment in the ionic residue. The Gailitis-Damburg analysis determines this dipole moment using first-order degenerate perturbation theory,[9,11] keeping terms in the large-r_e Hamiltonian of order $1/r_e^2$. This operator is represented as

$$A=\frac{l_e^2+2\mathbf{r}_i\cdot\hat{\mathbf{r}}_e}{2r_e^2}\ , \tag{1}$$

which for the $L=1$ odd parity final state has $2n-1$ eigenvectors related to Stark-type eigenstates of the residual hydrogenic ion $He^+(n)$. The five-dimensional operator A can be diagonalized in the representation consisting of radial hydrogenic wave functions $R_{nl_i}(r_i)$ multiplied by standard coupled spherical harmonics,

$$y_{nl_el_i}(\hat{\mathbf{r}}_e,\mathbf{r}_i)=R_{nl_i}(r_i)Y_{l_el_iLM}(\hat{\mathbf{r}}_e,\hat{\mathbf{r}}_i)\ , \tag{2}$$

where

$$Y_{l_el_iLM}(\hat{\mathbf{r}}_e,\hat{\mathbf{r}}_i)=\sum_{m_em_i}Y_{l_im_i}(\hat{\mathbf{r}}_i)Y_{l_em_e}(\hat{\mathbf{r}}_e)\times\langle l_em_e,l_im_i|LM\rangle\ . \tag{3}$$

The term in Eq. (1) which represents the photoelectron centrifugal barrier potential is diagonal in the representation of Eq. (2). The dipole-interaction term is off-diagonal,

$$\langle l_e'l_i'LM|\mathbf{r}_i\cdot\hat{\mathbf{r}}_e|l_el_iLM\rangle=R_{nl_i}^{nl_i'}\langle l_e'l_i'LM|\cos(\theta_{ie})|l_el_iLM\rangle\ , \tag{4a}$$

where θ_{ie} is the interelectronic angular separation,

$$R_{nl_i}^{nl_i'}\equiv\langle nl_i'|r_i|nl_i\rangle=-(3/2Z)n(n^2-l_>^2)^{1/2}$$

is the hydrogenic radial matrix element of r_i, Z is the nuclear charge, and $l_>$ is the larger of l_i and l_i'.[12] The matrix element of $\cos(\theta_{ie})$ in the coupled scheme is then [see equations (7.1.6) and (5.4.6) of Edmonds[13] with $k=1$]

$$\langle l_e'l_i'LM|\cos(\theta_{ie})|l_el_iLM\rangle=(-1)^{l_i'+l_i+L}[(2l_i+1)(2l_i'+1)(2l_e+1)(2l_e'+1)]^{1/2}\begin{Bmatrix}L & l_i' & l_e'\\ 1 & l_e & l_i\end{Bmatrix}\begin{bmatrix}l_e & 1 & l_e'\\ 0 & 0 & 0\end{bmatrix}\begin{bmatrix}l_i & 1 & l_i'\\ 0 & 0 & 0\end{bmatrix}. \tag{4b}$$

The final-state wave function in the asymptotic region for the channels associated with $He^+(n)$ can in general be written as

$$\Psi\rightarrow\sum_\alpha F_\alpha(r_e)\sum_{l_el_i}R_{nl_i}(r_i)Y_{l_el_iLM}(\hat{\mathbf{r}}_e,\hat{\mathbf{r}}_i)C_{l_el_i,\alpha}^{nL}\quad\text{as } r_e\rightarrow\infty\ , \tag{5}$$

where $C_{l_el_i,\alpha}^{nL}$ represents the eigenvector corresponding to the αth eigenvalue of the operator A in Eq. (1) with the sum occurring over all $(2n-1)$ dipole channels α. Exchange is irrelevant in the asymptotic region $r_e\rightarrow\infty$ and will be ignored, though its short-range effects are implicitly incorporated.

Equation (5) describes the escape of an electron from a hydrogenic ion as a superposition of all the physically allowed dipole channel functions with expansion coefficients $F_\alpha(r_e)$ which could in principle be numerically evaluated (see, e.g., Ref. 14). The major simplifying assumption here, as in Ref. 5, is that in two-electron photoabsorption processes only a single dipole channel α is dominantly excited out of the $(2n-1)$ available channels. This conclusion is supported by the hyperspherical potential curves[15,16] of H^- which reveal that photoemission from H^- or He occurs predominantly in the so-called "+" channel, the curve most attractive near the nucleus. For $^1P^0$ symmetry this corresponds approximately to the $T=1$, $K=n-1-T$ channels of Herrick.[6] Since this truncation to a single dominant channel rests on an adiabatic approximation,[15,16] it is only expected to be valid at low photoelectron energies, in particular for final-state energies lying just above the $He^+(n)$ threshold.

The final-state wave function can therefore be approximated with minimal error (see also Ref. 17) as the wave function of the single predominantly excited dipole channel,

$$\Psi_{KT}\rightarrow F_{KT}(r_e)\sum_{l_el_i}R_{nl_i}(r_i)Y_{l_el_iLM}(\hat{\mathbf{r}}_e,\hat{\mathbf{r}}_i)C_{l_el_i,KT}^{nL}\quad\text{as } r_e\rightarrow\infty\ , \tag{6}$$

where $(KT)\equiv\alpha$ with $K=n-1-T$ for the most attractive channel. This wave function was used in Ref. 5 to provide a simple derivation of a surprising result: photoionization via the $^1P^0$ final-state symmetry results in the ejection of photoelectrons normal to the direction of the external force, the photon polarization axis. This screw-type behavior was related to nonzero values of Herrick's SO(4) symmetry operator T^2. Heimann *et al.*[18] and Lin-

dle *et al.*[19] have since verified this prediction of orthogonal photoejection in helium, confirming the essential correctness of the approximations leading to Eq. (6). The elaborate variational calculation of Hayes and Scott[10] gives better quantitative agreement with experiment (at low n) than the analysis of Ref. 5, but its main conclusions are still valid.

B. Probability density

The alignment of the residual ion following a photon-atom "collision" is a particular type of collision-produced anisotropy. A simple measure of this anisotropy is obtained by calculating the ionic probability density. As with the photoelectron asymmetry parameter which completely describes the photoelectron angular distribution in the electric dipole approximation, the probability distribution of the ionic electron can also be characterized by a quadrupole asymmetry parameter.

The aforementioned asymptotic wave function Ψ_{KT} is used here to find the charge-cloud density after integrating over the ejected electron angular coordinates $\hat{\mathbf{r}}_e$,

$$\rho(\mathbf{r}_i) \propto \int |\Psi_{KT}|^2 d\hat{\mathbf{r}}_e = \sum_{\text{all } l\text{'s}} R_{nl_i}(r_i) R_{nl_i'}(r_i) C^{nL}_{l_e l_i, KT} C^{NL}_{l_e' l_i', KT} \times \int Y^*_{l_e' l_i' LM}(\hat{\mathbf{r}}_e, \hat{\mathbf{r}}_i) Y_{l_e l_i LM}(\hat{\mathbf{r}}_e, \hat{\mathbf{r}}_i) d\hat{\mathbf{r}}_e \ . \tag{7}$$

Equation (7) involves a coherent summation over the ionic electron orbital momenta and a sum over the photoelectron angular momenta which becomes incoherent owing to orthogonality of the spherical harmonics. The summation over magnetic quanta is carried out in terms of Wigner $3j$ and $6j$ coefficients, using Eq. (12) of Fano and Dill[4] or Eq. (2.20) of Rotenberg *et al.*[20] giving

$$\rho^{nL}_{KT}(\mathbf{r}_i) = \frac{9}{4\pi} \sum_{l_e l_i l_i'} (-1)^{l_e + l_i + l_i'} [(2l_i+1)(2l_i'+1)]^{1/2} R_{nl_i}(r_i) R_{nl_i'}(r_i) C^{nL}_{l_e l_i, KT} C^{nL}_{l_e l_i', KT} \times \sum_{k=0,2} (2k+1) \begin{pmatrix} l_i & l_i' & k \\ 0 & 0 & 0 \end{pmatrix} \begin{pmatrix} 1 & 1 & k \\ 0 & 0 & 0 \end{pmatrix} \begin{Bmatrix} 1 & 1 & k \\ l_i' & l_i & l_e \end{Bmatrix} P_k(\cos\theta_i) \ , \tag{8}$$

where $P_k(x)$ is the kth order Legendre polynomial of argument x.

It is readily seen that the integration of the $k=0$ term over the ionic electron coordinates is normalized to unity provided the Gailitis-Damburg eigenvectors are themselves normalized. Equation (8) can be cast into a more transparent form after dividing by the $k=0$ component giving the θ_i dependence of the density in the form

$$\rho^{nL}_{KT}(\mathbf{r}_i) \propto 1 + \beta(r_i) P_2(\cos\theta_i) \ , \tag{9}$$

where $\beta(r_i)$ contains a coherent summation over l_i and an incoherent sum over l_e.

A good measure of the ionic electron anisotropy is provided by the following "weighted" asymmetry parameter $\tilde{\beta}_{KT}$, defined by

$$\tilde{\beta}_{KT}(n) = \frac{\int r_i^2 \beta(r_i) \rho_0(r_i) dr_i}{\int r_i^2 \rho_0(r_i) dr_i} \ , \tag{10}$$

where $\rho_0(r_i)$ is the $k=0$ term in Eq. (8). This ionic electron asymmetry parameter characterizes the radially integrated probability density according to

$$\tilde{\rho}^{nL}_{KT}(\theta_i) = 1 + \tilde{\beta}_{KT}(n) P_2(\cos\theta_i) \ , \tag{11}$$

where θ_i represents the angle between the ionic electron radial axis and the photon polarization vector $\hat{\boldsymbol{\epsilon}}$. The ionic electron probability distribution thus exhibits the same quadrupole structure as the photoelectron angular distribution. In fact, one can anticipate the ionic electron probability cloud just below the Wannier threshold ($n \to \infty$) to align itself in the same manner as the photoelectron angular distribution, i.e.,

$$\tilde{\beta}_{KT}(n) = \begin{cases} -1, & T=1 \ (^1P^0) \\ 2, & T=0 \ (^3P^0) \end{cases} \tag{12}$$

at threshold.

This is confirmed for He in Fig. 1, which compares the photoelectron asymmetry parameter (from Ref. 5) to the ionic electron symmetry parameter as calculated using Eqs. (8) and (10) above. Figure 1 clearly demonstrates the one-to-one correspondence between the anisotropy in the photoelectron angular distribution and the hydrogenic electron probability distribution. This nearly identical behavior for the two asymmetry parameters becomes exact near the Wannier threshold, $n \to \infty$, where the two electrons have a tendency to stay on the opposite sides of the nucleus.[21] Photoionization of the $^1S^e$ ground state leading to a $^1P^0$ final-state energy just above a hydrogenic $He^+(n)$ threshold results in the alignment of the hydrogenic charge cloud *orthogonal* to the incident light polarization axis, while photoionization of the $^3S^e$ metastable state of He aligns the charge cloud *along* the field axis.

The opposite behavior of the two final-state symmetries can be partially interpreted on the basis of the two-electron angular separation θ_{ie}. Figure 2 gives an illustration of the dependence of the two-electron $^1P^0$ and $^3P^0$ wave functions on θ_{ie}.[22,23] The most important region of the configuration space for double-escape processes is the Wannier "saddle" region $\theta_{ie}=\pi$. Around $\theta_{ie}=\pi$ the two

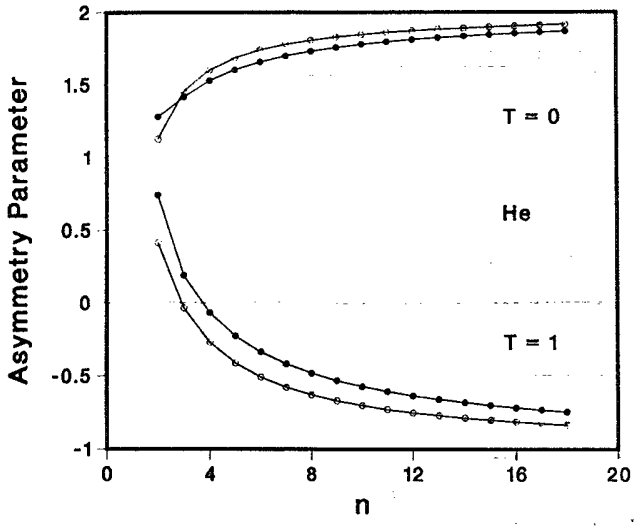

FIG. 1. Asymmetry parameters for the lowest energy photoelectrons (open circles, from Ref. 5) and the ionic electrons (closed circles) following photoionization of He are shown as a function of n, the principal quantum number of the residual He^+ ion. Shown are the asymmetry parameters for the two most dominant dipole channels $T=1$ ($^1P^0$) and $T=0$ ($^3P^0$). The final-state energy is assumed to lie just above the corresponding $He^+(n)$ threshold.

types of symmetry exhibit markedly different characteristics. The $^1P^0$ wave function almost vanishes at $\theta_{ie}=\pi$ while the $^3P^0$ wave function has a maximum at $\theta_{ie}=\pi$. The near vanishing of the $^1P^0$ ($T=1$) final state around the Wannier saddle effectively eliminates the main contribution from this particular final state to the ionization process, thus allowing for "unfavored" contributions to become dominant and the "unfavored" asymmetry parameter $\tilde{\beta}_{K(T=1)}\rightarrow -1$ to appear.[24]

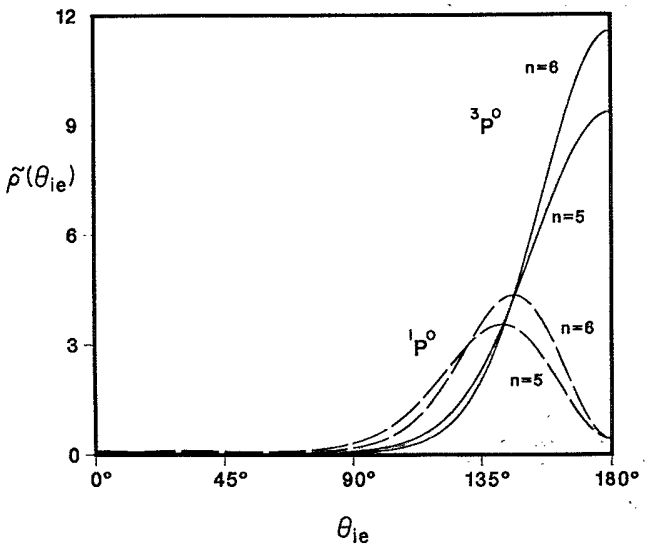

FIG. 2. Ionic electron probability density, averaged over the radial coordinate, is shown as a function of the interelectronic angular separation. The near, but incomplete, vanishing of the $^1P^0$ curves as $\theta_{ie}\rightarrow\pi$ is due to our assumption that the two electrons are at disparate radii, and hence not on the Wannier ridge.

Also interesting is the strong dependence of the ionic asymmetry parameter on the l_i coherence. If only the diagonal elements of the excited-state density matrix (i.e., $l_i=l_i'$) are considered, $\tilde{\beta}_{KT}$ obeys the expected "propensity rule" and remains positive for both types of final-state symmetry studied here. Propensity rules are approximate, even crude, "selection rules" which are usually based on classical arguments.[24] Accordingly, the expectation would be for the electrons to be distributed primarily along the direction of the incident electric dipole field. The coherence in l_i is quite essential for the alignment of the ionic electron orthogonal to the axis of quantization, i.e., $\tilde{\beta}_{K(T=1)}\rightarrow -1$, as in fact it can be shown that $\tilde{\beta}_{KT}\geq 0$ in the absence of this coherence for the parity-favored processes considered here.

C. Fluorescence intensity

Fano and Macek[2] showed that the alignment and orientation of collision fragments can be extracted by measuring the intensity and polarization of the fluorescence emitted by a fragment state. They expressed the intensity of the emitted light in terms of simple geometrical factors and a few dynamical parameters. These parameters are themselves related to the mean values of irreducible angular momentum operators. For the cylindrically symmetric configuration considered here, in which the collision frame has one axis of symmetry, the $q=0$ components of the orientation $O_q^{(1)}$ and the alignment $A_q^{(2)}$ are the only nonzero parameters,

$$O_0^{(1)}(l_i)=\frac{\langle L_{iz}\rangle}{\sqrt{l_i(l_i+1)}}$$

and (13)

$$A_0^{(2)}(l_i)=\frac{\langle 3L_{iz}^2-\mathbf{L}_i^2\rangle}{l_i(l_i+1)}\ ,$$

where the orientation parameter is normalized according to Ref. 3. Fano and Macek consider the alignment and orientation of a definite ionic angular momentum state l_i. As stressed in the Introduction, the angular momentum degeneracy of the hydrogenic levels, however, produces an interference effect for the different excitation amplitudes contributing to the alignment and/or circulation of the residual state in exactly the same way indistinguishable quantum-mechanical pathways leading to the same final-state interfere.

Since the photoelectron is assumed to remain unobserved, the total intensity of ionic fluorescence must be integrated over its angular coordinates. The resulting expression is

$$I\propto\int\sum_f|\langle\Psi_{KT}|(\hat{\epsilon}\cdot\mathbf{r})|\Psi_f\rangle|^2 d\hat{\mathbf{r}}_e\ , \tag{14}$$

where the incoherent summation occurs over the final states ($f\equiv l_f m_f$) which are, in principle, distinguishable. The polarization vector in the detector frame $\hat{\epsilon}$ is conveniently parametrized as $\hat{\epsilon}=(\cos\gamma, i\sin\gamma, 0)$, where γ replaces β of Ref. 2 to avoid confusion with the asymmetry parameters.

Substitution of the asymptotic wave function from Eq. (6) into Eq. (14) results in

$$I \propto \sum_f \int \langle \Psi_{KT}|(\hat{\epsilon}\cdot\mathbf{r}')|\Psi_f\rangle\langle\Psi_f|(\hat{\epsilon}^*\cdot\mathbf{r})|\Psi_{KT}\rangle d\hat{\mathbf{r}}_e$$
$$= \sum_{\text{all } l\text{'s}} \sum_{\text{all } m\text{'s}} \langle i|(\hat{\epsilon}\cdot\mathbf{r}')|f\rangle\langle f|(\hat{\epsilon}^*\cdot\mathbf{r})|i'\rangle\langle l_e m_e, l_i m_i|LM\rangle\langle LM|l_e m_e, l_i' m_i'\rangle C^{nL}_{l_e l_i, KT} C^{nL}_{l_e l_i', KT} , \quad (15)$$

where the integral over the photoelectron coordinates gives states of definite angular momenta l_e and their projections onto the quantization axis m_e. In Eq. (15) $|i\rangle$ and $|f\rangle$ represent hydrogenic excited and final states of the He^+. A recoupling transformation[25] brings the constant geometrical factors $\hat{\epsilon}$'s together to form a net kth rank multipole of the detected photon, giving as in Ref. 2,

$$\langle i|(\hat{\epsilon}\cdot\mathbf{r}')(\hat{\epsilon}^*\cdot\mathbf{r})P_f|i'\rangle = \sum_{k,q}(-1)^{k-q}[\epsilon^{(1)}\times\epsilon^{*(1)}]^{(k)}_q \times\langle i|[r'^{(1)}\times r^{(1)}]^{(k)}_{-q}P_f|i'\rangle , \quad (16)$$

where $P_f \equiv \sum_f |f\rangle\langle f|$.

To describe the angular distribution of the excited-state fluorescence, the polarization tensors $[\epsilon^{(1)}\times\epsilon^{*(1)}]^{(k)}_q$ must be transformed into the collision frame whose z axis coincides with the collision symmetry axis. This transformation through a set of Euler angles (ϕ,θ,χ) is performed using the relation[26]

$$T^{(k)}_q(\text{col}) = \sum_{q'} T^{(k)}_{q'}(\text{det})[D^{(k)}(\phi,\theta,\chi)]^{-1}_{q',q} . \quad (17)$$

The relevant polarization tensors in the collision frame are

$$[\epsilon^{(1)}\times\epsilon^{*(1)}]^{(0)}_0 = -3^{-1/2} ,$$
$$[\epsilon^{(1)}\times\epsilon^{*(1)}]^{(1)}_0 = 2^{-1/2}\sin(2\gamma)\cos\theta , \quad (18)$$
$$[\epsilon^{(1)}\times\epsilon^{*(1)}]^{(2)}_0 = -6^{-1/2}[P_2(\cos\theta) - \tfrac{3}{2}\cos(2\gamma)\sin^2\theta\cos(2\chi)] ,$$

whereas the nonvanishing elements of the polarization tensors in the detector frame are given in Ref. 27. In the preceding equations, circularly polarized light with a positive helicity has $\gamma=\pi/4$ and linear polarization translates into $\gamma=0$. In Eq. (18), the angle of the detector position relative to the collision symmetry axis is θ, and the orientation of a linear polarizer relative to the plane of the detector and the symmetry axis is χ.[2,3]

A common experimental setup for detecting linearly polarized fluorescence is to place the light detector at $\theta=\pi/2$ normal to the collision axis. Linear polarization is then defined as $P_L=(I_\parallel - I_\perp)/(I_\parallel + I_\perp)$, where $I_\parallel$ and $I_\perp$ represent the detected light intensities at the linear polarizer settings $\chi=0$ and $\chi=\pi/2$, respectively. Detection of circularly polarized fluorescence can be performed at the magic angle $\theta=54.7°$. Circular polarization is now defined as $P_C=(I_+ - I_-)/(I_+ + I_-)$, where I_+ and I_- are the transmitted intensities of the detected photons through the polarizers with positive and negative helicity, respectively.

The final expression for the intensity of the emitted light in the collision frame is obtained following the summation over the magnetic quanta in the usual form (e.g., see Eq. 2.20 of Rotenberg *et al.*[20]),

$$I = \frac{9}{4\pi} S \sum_{\text{all } l\text{'s}} X^{nLM}_{KT}(n_f,l_e,l_i,l_i',l_f) \sum_{k=0}^{2}(2k+1)^{1/2}[\epsilon^{(1)}\times\epsilon^{*(1)}]^{(k)}_0 \begin{bmatrix} L & L & k \\ -M & M & 0 \end{bmatrix} \begin{Bmatrix} 1 & 1 & k \\ l_i' & l_i & l_f \end{Bmatrix} \begin{Bmatrix} L & L & k \\ l_i' & l_i & l_e \end{Bmatrix} , \quad (19a)$$

with

$$X^{nLM}_{KT}(n_f,l_e,l_i,l_i',l_f) = (-1)^M(2l_f+1)[(2l_i+1)(2l_i'+1)]^{1/2} C^{nL}_{l_e l_i, KT} C^{nL}_{l_e l_i', KT} R^{n l_i}_{n_f l_f} R^{n_f l_f}_{n l_i'} \begin{bmatrix} 1 & l_f & l_i \\ 0 & 0 & 0 \end{bmatrix} \begin{bmatrix} 1 & l_f & l_i' \\ 0 & 0 & 0 \end{bmatrix} , \quad (19b)$$

where the constant of proportionality S in Eq. (19a) contains the dependence on the photoelectron radial wave function and the radiative transition frequency $\omega^4_{nn_f}$.

Equations (19) show that the coherence in l_i makes it impossible to extract the final-state contribution to the anisotropic light emission in the form of Fano-Macek-type geometrical factors $h^{(k)}(l_i,l_f)$, which are independent of the fragmentation dynamics. [The sums in Eqs. (19) can be evaluated analytically for a special case when the Gailitis-Damburg eigenvectors $C^{nL}_{l_e l_i, KT}$ are replaced with the Herrick SO(4) eigenvectors[6] which are pure geometrical vector coupling factors. Gailitis-Damburg eigenvectors have been shown,[5,17] however, to better represent the long-range effects of the short-range correlations between the photoelectron and the residual ion.] Note also that the only multipole moment in Eqs. (19) which depends on coherence in l_i is the "effective alignment" (A_{eff}), defined as the ratio of the coefficient in

front of the polarization tensor in the $k=2$ multipole term to the isotropic intensity (i.e., $k=0$ term). (Recall that, for a given l_e and l_f, l_i and l_i' are either both even or both odd.) This information enables us to calculate the orientation parameter $O_0^{(1)}(l_i)$ from the $k=1$ term in Eqs. (19) for a specific ionic angular momentum state. (The rank of the orientation and alignment parameters will subsequently be dropped for simplicity.)

Consequently, we show in Fig. 3 the alignment and orientation of $He^+(np)$ excited in He photoionization. Note that since the decay of an np excited state to the He^+ ground state displays no coherence in l_i, the polarized fluorescence is characterized by the Fano-Macek

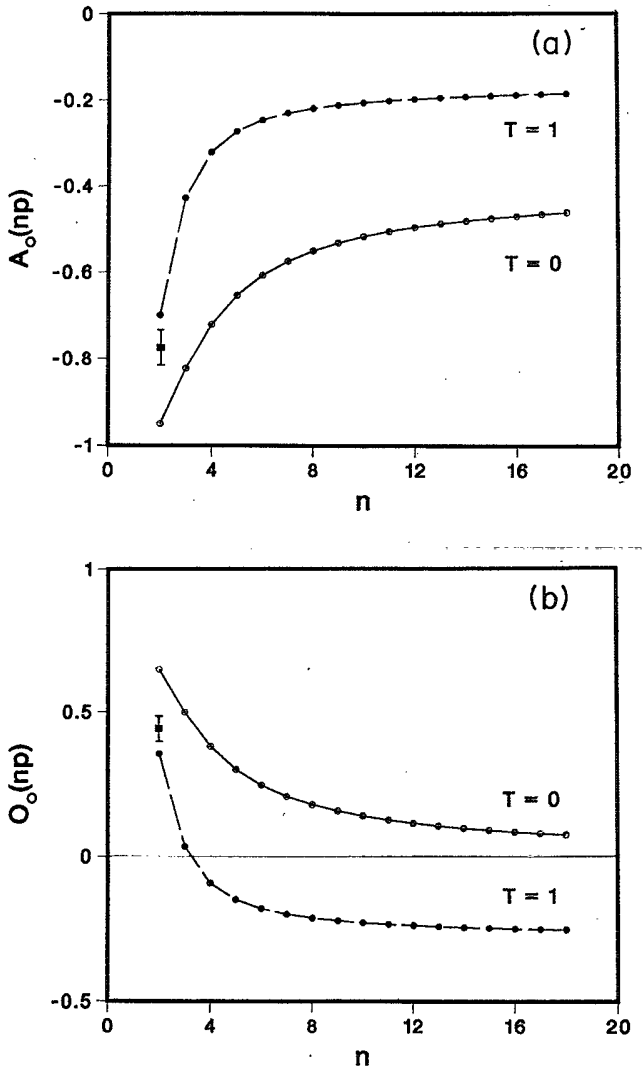

FIG. 3. Anisotropy parameters for the excited $He^+(np)$ states decaying to the He^+ ground state. The measured values of $A_0(2p)$ and $O_0(2p)$ deduced after correcting the experiment of Ref. 27 for depolarization effects are shown as closed squares in (a) and (b), respectively. Negative values of $O_0(np)$ characteizing the He^+-ion anisotropy following ionization by left-circularly polarized photons imply emission of opposite helicity fluorescence upon the radiative decay of a $He^+(np)$ excited state.

alignment $A_0(np)$ and orientation $O_0(np)$, parameters. Figure 3(b) reveals that for photoionization into the $^1P^0$ ($T=1$) final state, the $O_0(np)$ parameter is negative as the double-ionization limit is reached much the same way the electron asymmetry parameter $\tilde{\beta}_{K(T=1)}(n)$ was negative for $^1P^0$. It is mildly surprising that circular polarization of the detected fluorescence is predicted to have a sign opposite to that of the incident photon helicity. Despite the apparent violation of angular momentum conservation, this is possible if the photon angular momentum is primarily carried away by the photoelectron. The $^3P^0$ ($T=0$) symmetry, however, shows the expected behavior in agreement with the propensity rule[24] (see Sec. II C). The emitted fluorescence therefore possesses a helicity in the same direction as the incident photon helicity for $T=0$. The same propensity argument likewise suggests that the ionic electron density should "normally" align itself along the direction of the incident force field. In fact, we observe that the alignment parameter $A_0(np)$ obeys this rule for *both* final-state symmetries, i.e., $^1P^0$ and $^3P^0$. This agreement appears to be associated with the absence of coherence in l_i for the decay to the ground state. Recall that this l_i coherence was partly responsible for the observed trend toward $\beta \to -1$ shown in Fig. 1. It should be pointed out that the Herrick SO(4) eigenvectors do not give the $n \to \infty$ limiting values of $A_0(np)$ and $O_0(np)$ in Figs. 3(a) and 3(b), whereas they do correctly describe the limiting values of the photoelectron asymmetry parameter in Ref. 5.

Also shown in Fig. 3 are the measured values of $A_0(2p)$ and $O_0(2p)$ deduced from the experiment of Jimenez-Mier *et al.*,[28] after correcting for depolarization effects. Since no orientation measurements were made, we deduced the experimental value for $O_0(2p)$ from the branching ratio $\sigma(2p\epsilon s)/\sigma(2p\epsilon d)$ presented by Table I of Ref. 28. Our calculated results agree with these "measured" values reasonably well. The close-coupling analysis of Ojha,[29] however, gives this ratio to within the experimental uncertainty.

The dependence of $O_0(nl_i)$ on the orbital momentum l_i is given in Fig. 4, showing two noticeable patterns. First, the $^1P^0$ ($T=1$) final-state-symmetry curves increase quite regularly with l_i for increasing principal quantum number n. The orientation parameter is negative for this particular symmetry class for l_i less than some l_{max}. Rau[30] demonstrated that the probability for the excitation of l_i states in high doubly excited systems peaks at some $l_{max} \simeq \frac{1}{2}n^{1/2}$. The fact that the orientation is negative for $l_i \leq l_{max}$ requires (by angular momentum conservation) that the angular momentum of the incident photon is carried away by the unobserved photoelectron, e.g., the $l_e = l_i + 1$ channels are predominantly excited. The orientation curves for $^3P^0$ symmetry, on the other hand, obey the propensity rule $O_0(nl_i) > 0$ in the same region, $l_i < l_{max}$.[24] The second result is that in the region where the probability for the excitation of l_i states is exponentially low, the orientation parameter for both classes of symmetry converges to a limiting value of $\frac{1}{2}$. The "universal orientation" parameters of Ref. 3 give $O_0(l_i, l_e) \to \pm\frac{1}{2}$ as $l_i \to \infty$ for the parity favored branches[3]

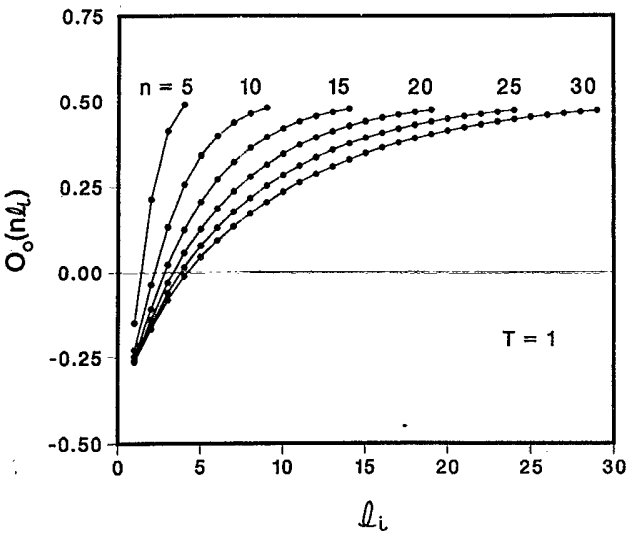

FIG. 4. "Partial" orientation parameters $O_0(nl_i)$ are given for the different excited nl_i states, displaying the anisotropy of individual orbital states.

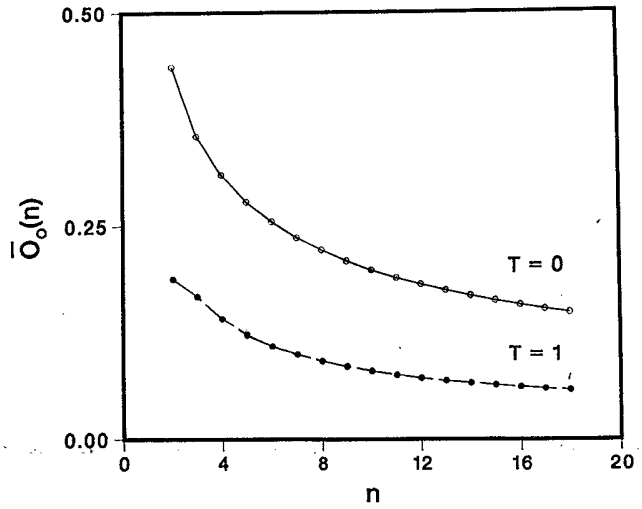

FIG. 5. "Weighted" orientation parameter from Eq. (20) shows the admixture of high nl_i levels producing a similar trend for $T=0$ and 1 final-state symmetries.

$l_e=l_i\mp1$. This realization and the prediction that $O_0(nl_i)\to\frac{1}{2}$ as $l_i\to\infty$ indicate that for large l_i there is substantial probability for the population of $l_e=l_i-1$ channels in contrast to the excitation of $l_e=l_i+1$ channels where $l_i<l_{\max}$.

States of high l_i are most efficiently populated close to the Wannier threshold.[31] This implies that near the double-escape threshold the admixture of these high nl_i states is expected, from preceding arguments, to cause the orientation parameter to exhibit a similar trend for both final-state symmetries. In fact, a "net orientation parameter" $\bar{O}_0(n)$, defined by

$$\bar{O}_0(n)=\frac{\sum_{l_i}\sigma(nl_i)O_0(nl_i)}{\sum_{l_i}\sigma(nl_i)}, \tag{20}$$

where $\sigma(nl_i)$ is the partial excitation cross section, shows that both symmetries $^1P^0$ and $^3P^0$ follow the same trend and are always positive throughout (see Fig. 5).

It is also evident from Eqs. (19) that the "effective alignment" A_{eff} plotted against n for decays of $n\to n-1$ in Fig. 6, depends on the coherent contributions of different l_i's. Even though both the dynamical and geometrical information stored in this term are intertwined by the coherence in l_i, some interesting observations can still be offered. The same general trend is also observed for small Δn decays ($\Delta n\sim1$–5). The $^1P^0$ ($T=1$) final-state curves become positive as $n\to\infty$, implying an alignment of the ionic electron orthogonal to the direction of the oscillating electric field of the incident light. $A_0(np)$ in Fig. 3(a) on the other hand remains negative for all n.

Note as well that this "effective quadrupole alignment" term remains negative for both classes of symmetry for those transitions having $\Delta n=n-n_f$ large. The importance of l_i coherence in producing these effects will be elaborated on more in the context of "depolarization" in the following section (Sec. II D).

D. Quantum beats and depolarization effects

Quantum beats are oscillatory time dependences which result from the coherent decay of nondegenerate excited fragment states j_i to different final states. The frequencies of these quantum beats for the problem at hand are $\omega_{j_ij_i'}=(E_{nl_i'j_i'}-E_{nl_ij_i})\hbar$, which for He^+ derive from fine structure and the Lamb shift, are roughly 10^{11} Hz for $n\sim2$, i.e., much faster than the typical experimental time resolution. For time-unresolved measurements the oscillatory time dependence $\exp(i\omega_{j_ij_i'}t)$ is replaced by

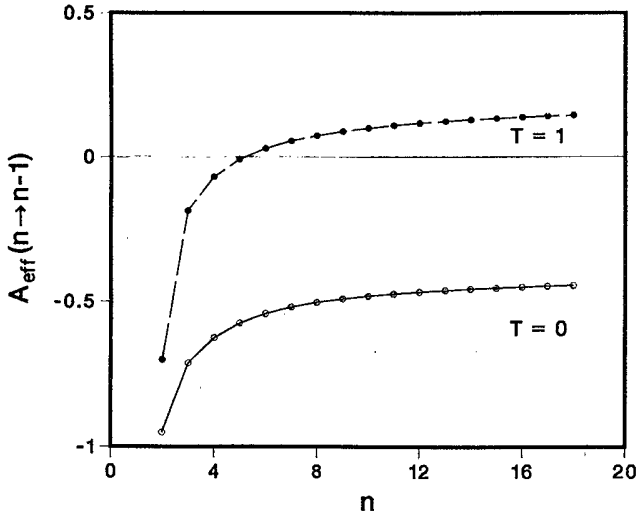

FIG. 6. "Effective alignment" parameter defined in Eqs. (19) showing small alignment orthogonal to the direction of the incident oscillating dipole field for $T=1$ symmetry.

$[1+(\omega_{j_i j_i'}\tau_i)^2]^{-1}$, in which τ_i is the decay lifetime for a hydrogenic l_i state.[12] This factor has a depolarizing effect on the total anisotropy in much the same way $h^{(k)}(l_i,l_f)$ is a measure of information lost when the final states are not observed. It affects the anisotropic intensity of the emitted fluorescence as follows: (1) if $\omega_{j_i j_i'}\tau_i \gg 1$, then there is a large depolarization of the total anisotropy and all off-diagonal terms with $j_i' \neq j_i$ are negligible, and (2) if $\omega_{j_i j_i'}\tau_i \ll 1$, then the "depolarization" factor reduces to unity and there will be little depolarization.[3]

The inclusion of fine-structure modulations in the total fluorescence intensity parallels the derivation of Sec. II C. The starting point is the frame-transformed asymptotic wave function used in Sec. II C, e.g., Eq. (6), with the oscillatory time dependence $\exp(iE_{nl_i j_i}t)$. Recoupling transformations of the kinds performed in Sec. II C, are also useful here. The matrix elements of the dipole tensors between jj-coupled initial and final states, e.g.,

$$\langle n(sl_i)j_i m_{j_i}|r_q^{(1)}|n_f(sl_f)j_f m_{j_f}\rangle ,$$

are reduced to products of standard coupling coefficients and reduced-dipole matrix elements [see equation (7.1.8) of Edmonds[13]].

The final expression for the total intensity including both the fine structure and l_i coherences in the collision frame is

$$I=\frac{9}{4\pi}S\sum_{\text{all } l\text{'s}}\sum_{\text{all } j\text{'s}}\langle(\tfrac{1}{2}\tfrac{1}{2})S,(l_e l_i)L|(\tfrac{1}{2}l_e)j_e,(\tfrac{1}{2}l_i)j_i\rangle^{(1)}\langle(\tfrac{1}{2}l_e)j_e,(\tfrac{1}{2}l_i')j_i'|(\tfrac{1}{2}\tfrac{1}{2})S,(l_e l_i')L\rangle^{(1)}$$
$$\times Q_{KT}^{nLM}(n_f,l_e,l_i,l_i',l_f,j_e,j_i,j_i',j_f)$$
$$\times\sum_{k=0}^{2}(-1)^k(2k+1)^{1/2}[\epsilon^{(1)}\times\epsilon^{*(1)}]_0^{(k)}\begin{bmatrix}1 & 1 & k\\ M & -M & 0\end{bmatrix}\begin{Bmatrix}1 & 1 & k\\ j_i' & j_i & j_e\end{Bmatrix}\begin{Bmatrix}1 & 1 & k\\ j_i' & j_i & j_f\end{Bmatrix}e^{i\omega_{j_i j_i'}t}, \qquad (21)$$

where

$$Q_{KT}^{nLM}(n_f,l_e,l_i,l_i',l_f,j_e,j_i,j_i',j_f)=(-1)^{j_f-j_e+j_i'+j_i}(2j_f+1)[(2j_i+1)(2j_i'+1)]^{1/2}X_{KT}^{nLM}(n_f,l_e,l_i,l_i',l_f)$$
$$\times\begin{Bmatrix}1 & l_f & l_i\\ \frac{1}{2} & j_i & j_f\end{Bmatrix}\begin{Bmatrix}1 & l_f & l_i'\\ \frac{1}{2} & j_i' & j_f\end{Bmatrix},$$

with S and $X_{KT}^{nLM}(\ )$ defined in Eqs. (19). If the oscillations cannot be resolved in time, each exponential factor must be replaced by the time-averaged "depolarization" factor. In Eq. (21) the fine-structure frequency is approximately proportional to $Z^4 n^{-3} l_i^{-2}$, where Z is the ionic charge.[12] The radiative lifetime τ_i, which is assumed the same for both values of $j_i = l_i \pm \frac{1}{2}$, is proportional to $n^3 Z^{-4}$.[12] Using the additional fact that τ_i is approximately proportional to l_i^2, this produces a product $(\omega_{j_i j_i'}\tau_i)$ roughly independent of Z, n, and l_i. Since the excited states of $He^+(nl_i)$ have decay lifetimes of about 10 ns, this product is usually much larger than unity reducing the "depolarization" factor to zero and effectively eliminating the fine-structure coherence which produced the quantum oscillations.

Polarization data calculated using Eq. (21) in Fig. 7 lend support these arguments. Polarization of the fluorescence detected following the decay of an excited state to $n_f=3$ is shown. The transition frequencies are so chosen as to be experimentally accessible (1.5×10^4 -4.5×10^4 cm^{-1}) in the visible and uv range. Figures 7(a) and 7(b) which give the linear polarization $[P_L=-3A_{\text{eff}}/(2-A_{\text{eff}})]$ for the $T=0$ and 1 final-state symmetries demonstrate that the precession of l_i and j_i is so rapid as to destroy the l_i coherence in addition to the fine-structure coherence. The depolarization effect is different for the two different symmetries. This can be partially traced to the Gailitis-Damburg eigenvectors $C_{l_e l_i,KT}^{nL}$ which give the probability amplitude for the excitation of an $(nl_i,\epsilon l_e)$ state. The quantum-mechanical processes leading to a final state $(n_f l_f)$ from these collision-excited states interfere differently for the $T=0$ and 1 final states. In fact, we see that the coherent product

$$C_{l_e l_i,K(T=1)}^{nL}C_{l_e l_i',K(T=1)}^{nL}$$

is positive producing an enhancement of the "unfavored" behavior which also materialized in $\tilde{\beta}_{K(T=1)}(n)$, see Fig. 1. The l_i coherence causes an orbital angular momentum "depolarization" in this case which tends to "pull" the polarization curve down. By including the fine-structure depolarization factor and $\omega_{j_i j_i'}\tau_i \gg 1$ the l_i coherence is "washed out" and the polarization curve for this class of symmetry is raised. For purposes of illustration the linear polarization calculated from Eq. (19) with $l_i=l_i'$ is shown also in Figs. 7(a) and 7(b).

The circular polarization curves of Fig. 7(c) show the expected trend. In contrast to Fig. 3(b), the circular po-

larization is positive for all n for decays of $n \rightarrow 3$. This is to be expected since the polarization data in Fig. 8(c) is a weighted sum of all excited angular momentum states decaying to the $n_f = 3$ final state. The admixture of these nl_i states produces a similar trend for both final-state symmetries $^1P^0$ and $^3P^0$ (see also Fig. 5).

The interplay of the coherence effects is also evident in the calculated linear polarization of the fluorescence detected following decays to $n_f = n - 1$ states shown in Fig. 8 (see also Fig. 6). Again, the "enhancement" effect caused by the l_i coherence is evident here as $T = 1$ the polarization curve becomes progressively negative as highly excited states n decay radiatively in the infrared. This apparently suggests an "unfavored" behavior as seen above in connection with the ionic asymmetry parameter of Fig. 1. The effect of fine-structure depolarization on both $T = 0$ and 1 final states is seen here to bring the two depolarized curves together. With the elimination of strong l_i coherence, which produced a "cancellation" effect for the $T = 0$ case and an "enhancement" effect for the $T = 1$ final state, the two symmetries are seen to have nearly the same polarized fluorescence, when not resolved in time.

III. SUMMARY

In this paper we examine the anisotropy of excited states of He^+ ions following photoionization of He. (Similar predictions can be readily made for H^- as well.)

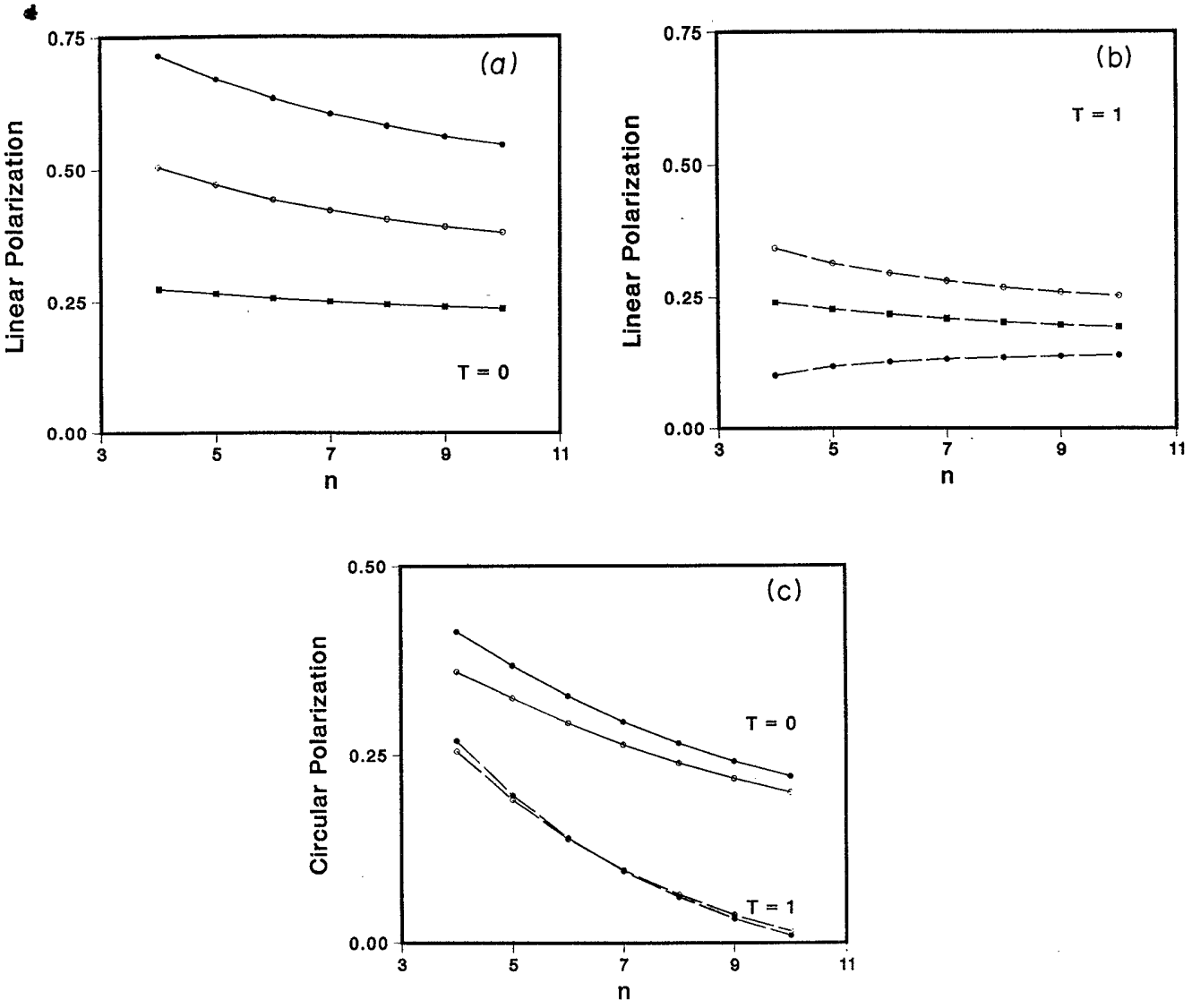

FIG. 7. Predicted (dimensionless) polarization of the fluorescence emitted upon $n \rightarrow n_f = 3$ level transitions is shown as a function of n. (a) and (b) give the linear polarization for $T = 0$ and 1, respectively. Results shown with closed circles include the l_i-coherence effects; open circles are given for illustrative purposes with this coherence aritifically taken out; and closed squares include the full effect of fine-structure depolarization. Note the large effect of depolarization on these time-unresolved anisotropies. (c) shows the circular polarization of the detected fluorescence for the same transitions as in (a) and (b) with the open (closed) circles characterizing the anisotropy with (without) the inclusion of fine-structure depolarization.

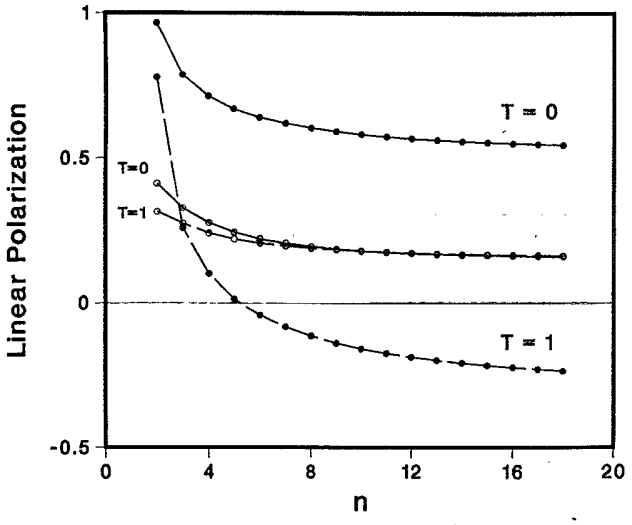

FIG. 8. Dimensionless linear polarization of the fluorescence for $n \rightarrow n-1$ decay transitions is predicted as a function of n. The effect of l_i coherence, included in the results shown with closed circles, on the alignment of the ionic electron is strongly evident here. This coherence is eventually destroyed by including the fine-structure depolarization, represented by open circles, as would be observed in a typical time-unresolved experiment.

The effect of the orbital momentum coherence of degenerate hydrogenic states on the anisotropy parameters is quantitatively studied. In the first part of this article, the Ref. 5 treatment of single photoelectron angular distribution for two-electron systems is extended to describe the properties of the residual ionic electron. By casting the expression for the charge density in the same form as the photoelectron differential cross section $d\sigma/d\Omega \propto 1+\beta(n)P_2(\cos\theta)$, we are able to define an asymmetry parameter $\tilde{\beta}_{KT}(n)$ for the electronic charge distribution. For two classes of final-state symmetry, $^1P^0$ and $^3P^0$, $\tilde{\beta}_{KT}(n)$ mimics the behavior of the photoelectron asymmetry parameter as a function of n. This one-to-one correspondence results because the asymptotic "dipole" channels reflect the short-range pattern of electron correlations even at very large photoelectron distances, $r_e \rightarrow \infty$.

The Fano-Macek-type anisotropy parameters, the alignment and orientation of the excited ionic state, are calculated with the intention of studying the effect of l_i coherence on these parameters. The orientation parameter is automatically independent of the coherence in l_i owing to parity and angular momentum conservation. The calculation of $A_0(np)$ and $O_0(np)$ produces some surprising results. The detected circular polarization following the decay of an (np) level is seen to have the opposite sign of the incident light circular polarization, for high-lying states of the He^+ ion. The alignment parameter for the same final-state symmetry, namely, $^1P^0$ $(T=1)$, does not exhibit the same behavior. This is rather interesting in the sense that $\tilde{\beta}_{KT}(n)$, also a second rank multipole, shows opposite trends for the two final state classifications $^1P_0$ and $^3P^0$. This disparity between the two quadrupole anisotropy parameters is associated with the absence of l_i coherence in $A_0(np)$, since this coherence is strongly influential in producing the observed effects in the ionic asymmetry parameter. Agreement between theory and the only experimental data points for the $2p$ level is better than that between the theoretical value for $\beta(n=2)$ from the analysis of Ref. 5 and the experiment of Heimann *et al.*[18]

The dependence of the orientation parameter on individual orbital momentum state l_i is studied. Note that the orientation parameter $O_0(nl_i)$ is independent of the coherence in l_i allowing for its study (theoretically if not experimentally) as a function of orbital angular momentum. For the experimentally relevant case of the $T=1$ $^1P^0$ final state the orientation is negative for $l_i < l_{\max} = \frac{1}{2}n^{1/2}$ where the probability $\sigma(nl_i)$ peaks. For $l_i > l_{\max}$ instead, the orientation parameter is positive as typically expected.

Since the alignment parameter depends on coherence in l_i, an "effective alignment" parameter is introduced which includes both dynamical and geometrical information intertwined by the coherence. For the emission of low-frequency photons following the decay of excited states of He^+ this effective alignment parameter exhibits the same general trend as that for $\tilde{\beta}_{KT}(n)$ thereby confirming that the coherence in l_i is partly responsible for these unexpected observations.

Finally, the effect of the fine-structure depolarization on the anisotropy parameters is investigated. It is shown that the l_i coherence, which plays a strong role in predicting the linear polarization of the emitted light, influences the $T=0$ and 1 final-state symmetries quite differently but this difference is eventually "washed out" in any realistic time-unresolved measurements by fine-structure depolarization. Alternatively, effects of the l_i coherence could be observed in a time-resolved experiment with or without electric field present, as in the electron-hydrogen scattering experiments of Heck and Williams.[32]

ACKNOWLEDGMENT

This work was supported in part by a grant from the National Science Foundation.

[1]D. Dill and U. Fano, Phys. Rev. Lett. **29**, 1203 (1972).
[2]U. Fano and J. H. Macek, Rev. Mod. Phys. **45**, 553 (1973).
[3]C. H. Greene and R. N. Zare, Ann. Rev. Phys. Chem. **33**, 119 (1982); Phys. Rev. A **25**, 2031 (1982).
[4]U. Fano and D. Dill, Phys. Rev. A **6**, 185 (1972).
[5]C. H. Greene, Phys. Rev. Lett. **44**, 869 (1980); see also J. Phys. B **20**, L357 (1987).
[6]D. R. Herrick, Phys. Rev. A **12**, 413 (1975).
[7]G. Gabrielse, Phys. Rev. A **22**, 138 (1980).
[8]J. Burgdörfer, Z. Phys. A **309**, 285 (1983).

[9]M. Gailitis and R. Damburg, Proc. Phys. Soc. London **82**, 192 (1963).
[10]M. A. Hayes and M. P. Scott, J. Phys. B **21**, 1499 (1988), and references therein.
[11]M. J. Seaton, Proc. Phys. Soc. London **77**, 174 (1961).
[12]H. E. Bethe and E. E. Salpeter, *Quantum Mechanics of One- and Two-Electron Atoms*, 1st ed. (Plenum, New York, 1977).
[13]A. R. Edmonds, *Angular Momentum in Quantum Mechanics* (Princeton University Press, New Jersey, 1960).
[14]J. Macek and P. G. Burke, Proc. Phys. Soc. London **92**, 351 (1967).
[15]J. H. Macek, J. Phys. B **1**, 831 (1968).
[16]U. Fano, Rep. Prog. Phys. **46**, 97 (1983); C. D. Lin, Adv. At. Mol. Phys. **22**, 77 (1986).
[17]A. F. Starace and J. H. Macek, Phys. Rev. Lett. **58**, 2385 (1987).
[18]P. A. Heimann, U. Becker, H. G. Kerkhoff, B. Langer, D. Szostak, R. Wehlitz, D. W. Lindle, T. A. Ferrett, and D. A. Shirely, Phys. Rev. A **34**, 3782 (1986).
[19]D. W. Lindle, P. A. Heimann, T. A. Ferrett, and D. A. Shirley, Phys. Rev. A **35**, 1128 (1987).
[20]M. Rotenberg, R. Bivens, N. Metropolis, and J. K. Wooten, Jr., *The 3j- and 6j-Symbols* (MIT, Cambridge, MA, 1959).
[21]A. R. P. Rau, Atoms in Unusual Situations **143**, 383 (1985); Phys. Rep. **110**, 369 (1984).
[22]Figure 2 represents equation B5 of Ref. 23 as a function of the interelectronic angle θ_{ie} in the asymptotic limit $r_e \rightarrow \infty$, averaged over the ionic electron radial coordinate. As a first approximation the asymptotic wave function, Eq. (6), is used in place of the adiabatic wave function, equation B2 of Ref. 23, hence replacing the body-frame radial function

$$G_{l_e l_i}(R,\alpha) \rightarrow F(r_e) C^{nL}_{l_e l_i, KT} R_{nl_i}(r_i) ,$$

as $R \rightarrow \infty$.
[23]J. Botero, Phys. Rev. A **35**, 36 (1987).
[24]C. H. Greene, in *Fundamental Processes of Atomic Physics*, edited by J. S. Briggs, H. Kleinpoppen, and H. O. Lutz (Plenum, New York, 1988).
[25]U. Fano and G. Racah, *Irreducible Tensorial Sets* (Academic, New York, 1959).
[26]I. V. Hertel and W. Stoll, Adv. At. Mol. Phys. **13**, 113 (1977).
[27]C. H. Greene and R. N. Zare, J. Chem. Phys. **78**, 6741 (1983).
[28]J. Jimenez-Mier, C. D. Caldwell, and D. L. Ederer, Phys. Rev. Lett. **57**, 2260 (1986).
[29]P. C. Ojha, J. Phys. B **17**, 1807 (1984).
[30]A. R. P. Rau, J. Phys. B **17**, L75 (1984).
[31]U. Fano, J. Phys. B **7**, L401 (1974).
[32]E. L. Heck and J. F. Williams, J. Phys. B **20**, 2871 (1987).